Eur. Phys. J. B **47**, 29–35 (2005)
DOI: 10.1140/epjb/e2005-00297-9

THE EUROPEAN PHYSICAL JOURNAL B

Role of A-site deficiency in the magneto-transport properties of $Pr_{0.7}Sr_{0.3}MnO_3$ relaxed films

M. Koubaa[1,3], W. Prellier[2], R. Soulimane[1], W. Boujelben[3], A. Cheikh-Rouhou[3,a], Ph. Lecoeur[1], and A.-M. Haghiri-Gosnet[1]

[1] Institut d'Électronique Fondamentale, IEF - UMR 8622 CNRS, Bâtiment 220, Université Paris-Sud, 91405 Orsay Cedex, France
[2] Laboratoire de Cristallographie et Sciences des Matériaux, CRISMAT, CNRS UMR 6508, ENSICAEN, 6 boulevard du Maréchal Juin, 14050 Caen Cedex, France
[3] Laboratoire de Physique des Matériaux, Faculté des Sciences de Sfax, B.P. 802, Sfax, Tunisia

Received 1st October 2004 / Received in final form 25 February 2005
Published online 21 September 2005 –

Abstract. The magneto-transport properties of thick relaxed A-site deficient films having the composition $Pr_{0.6}\square_{0.1}Sr_{0.3}MnO_3$($P_\square SMO$ with the $\square$ symbol for the Pr vacancy) and $Pr_{0.7}Sr_{0.2}\square_{0.1}MnO_3$($PS_\square MO$) are studied. A direct comparison with a $Pr_{0.7}Sr_{0.3}MnO_3$(PSMO)completely relaxed film, deposited under the same growth conditions, shows a reduction of the in-plane parameter a_{100} associated to an enhancement of the out-plane parameter. The strains (bulk strain ε_B and biaxial Jahn-Teller strain ε_{J-T}) do vary with the nature of the cationic vacancy. For example, an enhancement of ε_B of 9% in the $PS_\square MO$ film (Sr deficient) produces a decrease of T_C of 30 K, whereas the Pr deficient $P_\square SMO$ film exhibits a large reduction of both $\varepsilon_B(-16\%)$ and ε_{J-T} (divided by a factor of 5), which enhances T_C of 12 K, similarly to previous observations on bulk ceramics. With a reduced resistivity ($\rho < 0.02\ \Omega\,$cm), the obtained Pr-deficient film, $P_\square SMO$, exhibits the best magneto-transport properties with a decreasing magnetoresistance sensitivity at low field.

PACS. 75.47.Lx Manganites – 75.50.-y Studies of specific magnetic materials – 75.70.-i Magnetic properties of thin films, surfaces, and interfaces

1 Introduction

The mixed-valence perovskites $R_{1-x}A_xMnO_3$, where R and A are rare earth and alkaline-earth elements, exhibit a metal-insulator transition accompanied by so-called colossal magnetoresistance (CMR) – an abnormal decrease of resistivity under the application of a magnetic field [1–4]. These oxides have a rich, complex and still under-debate physics that is related to the competing electron-lattice and electron-electron interactions. Their structural, magnetic and transport properties are thus intricately related. Several studies, both experimental and theoretical, have been performed by various groups. For example; Millis et al. [5,6] have proposed a dynamical mean-field model of Jahn-Teller (J-T) electrons coupled to "core spins" and to phonons for describing the CMR physics. Since the electron-phonon coupling is fully driven by the J-T effect that distorts the MnO_6 octahedral, several studies have attempted to modify this distortion either by means of an internal chemical pressure (change of the average ionic radius on both A and B sites from a chemical substitution) [7–9] or by means of an external pressure [10–12]. Since a well-controlled lattice distortion can easily be introduced in strained thin films due to the lattice mismatch between the single crystal substrate and the film, the strained films appear very useful to study and to drive the J-T distortion. Many research groups have reported systematic studies by using different substrates that induce different lattice mismatches and thus different lattice strains [13]. These experiments are well designed to probe the intrinsic effects of both competing hydrostatic and Jahn-Teller strains upon the magnetic and electric properties.

Strain effects can thus directly influence the physical properties of the manganites thin films including the Curie temperature (T_C), the magnetic anisotropy and the magneto-resistance (MR). While a tensile strain generally decreases T_C in (La,Sr)MnO_3 and (La,Ca)MnO_3 compounds deposited on $SrTiO_3$ (STO) due to a large J-T distortion, an anomalous increase of T_C has been observed in $La_{0.8}Ba_{0.2}MnO_3$ on STO tensile films due to a larger hydrostatic bulk term [14]. In compressive $Pr_{0.67}Sr_{0.33}MnO_3$ thin films grown on $LaAlO_3$ (LAO), the easy axis of magnetization is found to be perpendicular of the film's plane, inducing large anomalous low-field MR ($LFMR$) under perpendicular applied magnetic field [15,16].

In this paper, we propose an alternative way to introduce an additional lattice distortion in $R_{1-x}A_xMnO_3$

[a] e-mail: Abdel.Cheikhrouhou@fss.rnu.tn

films: the presence of a cationic vacancy on the A-site of the perovskite lattice cell. Previous studies on A-site deficient $Pr_{0.7}Sr_{0.3}MnO_3$ (PSMO) bulk ceramics have reported both an increase of T_C in Pr-lacunars compounds ($Pr_{0.7-x}\square_xSr_{0.3}MnO_3$ with $0.05 < x < 0.2$) [17], or a decrease of T_C in Sr-deficient $Pr_{0.7}Sr_{0.3-x}\square_xMnO_3$ (with $x \leq 0.2$) associated to a contraction of the unit cell [18]. In stoichiometric $Pr_{0.67}Sr_{0.33}MnO_3$ thin films, H.S. Wang et al. have studied the variation of the out-of-plane parameter c_{001} for thickness (t) ranging from a few nanometers to 300 nm. These authors have shown that the films thicker than 300 nm are fully relaxed, with a c_{001} value equal or even lower to the bulk parameter ($a_{P\,PSMO} = 3.867$ Å) [16]. In this study, thick relaxed films (thickness, $t = 450$ nm–600 nm) have been grown in order to minimize the strain component due to the substrate mismatch that always produce large cell distortion, in order to avoid surface effects of magnetic depolarization and thus to be able to extract the cell distortion produced only by vacancies. This work is a first step that will verify the ability to introduce vacancy in films and check the nature of the cell distortion mainly imposed by the vacancy.

The magnetic and transport properties of A-site deficient $Pr_{0.7}Sr_{0.3}MnO_3$ thick films deposited on LAO have been studied as a function of the nature of the vacancy and are reported in this paper. Measurements of the lattice parameters (in-plane a and out-plane c), the resistive transition T_P, the Curie point T_C, the high field MR ($HFMR$, with $HFMR = -CMR = -[R(8\text{ T}) - R(0\text{ T})]/R(8\text{ T})$) and the low field MR were performed on the stoichiometric $Pr_{0.7}Sr_{0.3}MnO_3$ (PSMO) films as well as on both lacunars $Pr_{0.6}\square_{0.1}Sr_{0.3}MnO_3$($P_\square SMO$) and $Pr_{0.7}Sr_{0.2}\square_{0.1}MnO_3$ films ($PS_\square MO$). Our results are discussed and compared to the results observed in bulk ceramics.

2 Experiment

The dense targets of PSMO, $P_\square SMO$ and $PS_\square MO$ were synthesized using standard ceramic methods. Pr_6O_{11},Mn_2O_3 and $SrCO_3$ powders of 99.9% purity were mixed in appropriate ratios and intimately ground using a semi-planetary ball mill. The mixed powder was first annealed at 1000 °C for 60 hours to ensure a complete reaction. The resulting powders were pressed into pellets (of about 2 mm thickness) and sintered at 1400 °C for 60 hours with intermediate grindings and repressing. Finally, these pellets were rapidly quenched at room temperature in air to retain the high temperature structure. Powder X-ray diffraction (XRD) analysis at room temperature shows single-phases that crystallize in a rhombohedral perovskite structure (for the parent PSMO compound as well as for the deficient $P_\square SMO$ and $PS_\square MO$).

The films were grown on (100) LAO substrate using a standard PLD apparatus [13] working with a KrF excimer laser at $\lambda = 248$ nm. The laser fluence was fixed at 1–2 J/cm^2 and the pulse rate at 2 Hz. Before deposition, the single-crystal LAO substrates were cleaned in ultrasonic baths of acetone and ethyl alcohol, and then were attached to the heater using silver paste. The heater can be translated for proper target-to-substrate positioning. A K-type thermocouple was mechanically attached to the heater block close to the substrate and the temperature measured at this location is referred to as the deposition temperature. The optimal deposition temperature was fixed at 675 °C for a dynamic O_2 pressure of 300 mTorr. After complete deposition, the films were cooled to room temperature at 20 °C/min under a static oxygen pressure of 500 mbar. X-ray diffraction patterns were recorded utilizing a SEIFERT 3000P in a standard $\theta-2\theta$ configuration for the out of plane measurements. In-plane measurements were carried out by using an X'Pert MRD diffractometer. The in-plane lattice parameter were obtained from the (103) reflection of the cubic unit cell, by tilting of an angle $\Psi(\Psi \approx 18°$ for 103 diffraction plane) in order to move this plane in the Bragg conditions and by scanning a normal Θ–2Θ around this reflection. The c-axis value (out-of-plane lattice parameter) is obtained from the $00l$ reflections of the routine Θ–2Θ scan (see Fig. 1 hereafter). Using this value and the following formula $d_{hkl} = 1/(h^2/a^2 + k^2/b^2 + l^2/c^2)^{(1/2)}$, we calculated the a-axis value (in-plane lattice parameter) with $h = 1$, $k = 0$ and $l = 3$.

The thickness (t) of the films was determined to be $t = 600$ nm for PSMO and $PS_\square MO$ and $t = 450$ nm for $P_\square SMO$, from profilometric measurements on etched patterns. The films used in this study are thicker than 300 nm and thus relaxed, as explained hereafter. A MPMS 5S super conducting quantum interference device magnetometer from Quantum Design was used in the temperature (T) range 4 K–300 K for determining the Curie temperatures (T_C). After a zero-field cool procedure, the coercivity (H_C) was deduced from the $m(H)$ curves at 4 K and the evolution of magnetization was measured on warming under 50 mT. The resistivity (ρ) was measured using a conventional in-line four-probe technique, with the voltage contacts aligned along (100) and spaced from 2 mm. The magnetic field (H) was applied along (100) and the dc current was fixed at 10 mA.

3 Structure

The XRD patterns (see Fig. 1) clearly evidenced that all the films of PSMO, $P_\square SMO$ and $PS_\square MO$ are single-phased with the 001 axis (referring to the cubic unit cell) perpendicular to the substrate plane. The films are well crystallized with in-plane alignment within the substrate plane (not shown). The calculated values obtained from XRD analysis are reported in Table 1.

The bulk manganite PSMO has a pseudocubic parameter $a_P = 3.867$ Å [19]. The lattice mismatch δ of PSMO on the LAO substrate, that has a smaller cell ($a_P = 3.788$ Å, pseudocubic), is $\delta = (a_{p\,substrate} - a_{p\,bulk})/a_{p\,substrate} = -0.02\%$. This negative mismatch describes a compressive stress: the cell should be elongated along the growth direction (with $c_{001} > a_{p\,bulk} = 3.867$ Å) and compressed in the

Table 1. The thin films crystallographic in-plane a_{100} and out-plane c_{001}parameters from XRD measurements. The perovskite parameter a_P of the bulk parent compound is also reported from [20] to allow determination of strains ε_{100} and ε_{001}. The bulk strain ε_B and the bi-axial J-T strain ε_{J-T} have been deduced for each film. Note that $P_{\square}SMO$ thin film exhibits a quite negligible ε_{001}value and thus a reduced J-T term.

	$Pr_{0.7}Sr_{0.3}MnO_3$	$Pr_{0.7}Sr_{0.2}\square_{0.1}MnO_3$	$Pr_{0.6}\square_{0.1}Sr_{0.3}MnO_3$
$a_P$bulk (polycrystalline)			
from [20]	3.867 Å	3.8643 Å	3.8618 Å
V_{bulk}– cell volume	57.82 Å^3	57.7 Å^3	57.59 Å^3
		($\Delta V/V = -0.2\%$)	($\Delta V/V = -0.39\%$)
In-plane parameter			
a_{100}	3.887 Å	3.880 Å	3.871 Å
In-plane distortion			
$\varepsilon_{100} = (a_{100} - a_P)/a_P$	5.17×10^{-3}	4.06×10^{-3}	2.38×10^{-3}
Out-plane parameter			
c_{001}	3.849 Å	3.857 Å	3.862 Å
Out-plane distortion			
$\varepsilon_{001} = (c_{001}$- $a_P)/\ a_P$	-4.65×10^{-3}	-1.89×10^{-3}	0.5×10^{-4} ($\sim$0)
V_{film}	58.15 Å^3	58.06 Å^3	57.87 Å^3
		($\Delta V/V = -0.15\%$)	($\Delta V/V = -0.48\%$)
Hydrostatic distortion			
$\varepsilon_B = 1/3(2\varepsilon_{100} + \varepsilon_{001})$	1.9×10^{-3}	2.08×10^{-3}	1.60×10^{-3}
Jahn-Teller distortion			
$\varepsilon_{J-T} = 1/2(\varepsilon_{001} - \varepsilon_{100})$	$\sim -5 \times 10^{-3}$	-3×10^{-3}	-1×10^{-3}

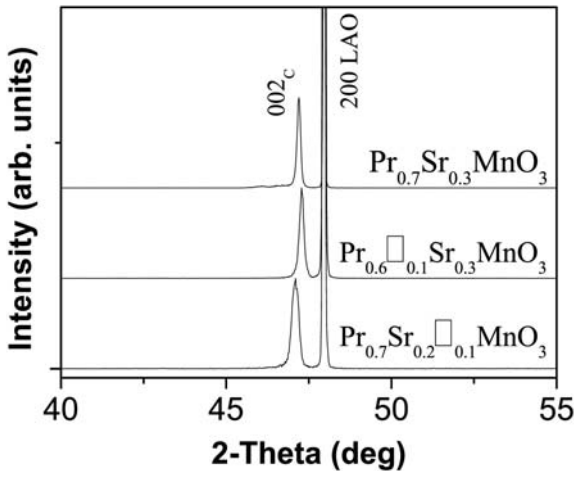

Fig. 1. X-ray diffraction patterns in a standard θ-2θ configuration for the out of plane measurements recorded on all the thick relaxed films (PSMO, $P_{\square}SMO$ and $PS_{\square}MO$) deposited on LAO. The low intensity feature observed in PSMO at $2\theta = 46^\circ$ is likely due to the presence of small domains with a [110]–orientation whereas most of the film is [001]–oriented (referring to the cubic unit cell).

plane of the film (with $a_{100} < a_{p\,bulk}$). In this case of a compressive stress, the perpendicular distortion ε_{001}, defined as $\varepsilon_{001(out-plane)} = (c_{001} - a_P)/a_P$, takes a positive value, whereas the in-plane distortion $\varepsilon_{100(in-plane)} = (a_{100} - a_P)/a_P$ is negative. On the opposite, a tensile film will exhibit a negative out-plane ε_{001} associated to a positive in-plane ε_{100}. Wang et al. have shown that the out-plane parameter c_{001} is decreasing from about 3.95 to 3.87 Å ($= a_{p\,bulk}$) when the thickness increases from a few nanometers to $t = 300$ nm [16]. The perpendicular distortion ε_{001} is thus approaching zero which expresses a full relaxation of the compressive stress in 300 nm-thick films. In our 600 nm-thick stoechiometric PSMO film, in agreement with Wang's results, the out-plane parameter c_{001} is reduced to 3.849 Å ($< a_{p\,bulk}$) and the corresponding in-plane parameter a_{100} is enhanced to 3.887 Å. From the Table 1, it is shown that the out-of-plane lattice parameters are slightly smaller as compared to the bulk indicating a small tensile stress within the plane of the substrate.

The small tensile stress observed in this very thick film is confirmed by the small negative value of the perpendicular distortion $\varepsilon_{001(out-plane)}$ ($\varepsilon_{001(out-plane)} = -4.65 \times 10^{-3}$). Note that a 20 nm-thick strained PSMO film exhibits a 10 times larger compressive distortion of about $\varepsilon_{001(out-plane)} = +18.9 \times 10^{-3}$, as calculated from Wang's data [16]. In our thick relaxed lacunars films, the lattice distortion is largely reduced ($|\varepsilon_{001}| < 5 \times 10^{-3}$) if compared to thin strained films. The role of the lattice distortion imposed by a *A*-site vacancy will be thus more easier to observe and to extract in these slightly distorted and relaxed films than in very thin strained films. From the strains $\varepsilon_{100(in-plane)}$ and $\varepsilon_{001(out-plane)}$, the bulk hydrostatic strain ε_B and biaxial J-T strain ε_{J-T} have been also calculated (see Tab. 1) [20]. Note that the bulk hydrostatic strain ε_B is always positive (with $2\varepsilon_{100} > -\varepsilon_{001}$),

whereas the biaxial J-T strain $\varepsilon_{\mathrm{J-T}}$ remains always negative.

A direct observation of the evolution of the lattice parameters a_{100} (in-plane) and c_{001} (out-of-plane)is of great interest: both P$_\square$SMO and PS$_\square$MO films exhibit a larger out-plane parameter associated to a smaller in-plane,with a reduced total cell volume (as compared to stoichiometric PSMO films. Such a decrease of the unit cell due to the presence of vacancies was previously observed in bulk polycrystalline P$_\square$SMO and PS$_\square$MO compounds [21]. The reduced values of both $\varepsilon_{100(\mathrm{in-plane})}$ and $\varepsilon_{001(\mathrm{out-plane})}$ distortions indicate also that the deficient films are less distorted and thus less stressed than the stoichiometric PSMO thick film. Note that ε_{001} is quite negligible for the P$_\square$SMO film. If the total volume is decreasing for both lacunars films, the hydrostatic distortion ε_{B} and the Jahn-Teller distortion $\varepsilon_{\mathrm{J-T}}$ are not varying similarly with the nature of the vacancy. In others words, with a Sr vacancy, ε_{B} is enhanced and $\varepsilon_{\mathrm{J-T}}$ is reduced. On the opposite, a Pr vacancy induces a more significant decrease of both ε_{B} and $\varepsilon_{\mathrm{J-T}}$ distortions, which is in favor of an enhancement of the Curie temperature. The role of each distortion upon T_C will be discussed hereafter.

4 Magnetic and electric transport properties of deficient thin films

4.1 Deficiency dependence of T_C

One of the most attracting features of the manganite is the occurrence of a resistive transition at T_{P} from a high temperature insulating phase towards a metallic one, which is close to the PM/FM Curie temperature T_C. The evolution of these temperatures has been studied as a function of the nature of the vacancy i.e. on the Sr or the Pr sites. Similarly to polycrystalline bulk materials [18], it is observed a decrease of both T_{P} and T_C in the Sr deficient PS$_\square$MO relaxed film, whereas the presence of a Pr deficiency shifts towards larger T_{P} and T_C temperatures. The resistivity curves $\rho(T)$ and the magnetization curves $m(T)$ are presented in the Figure 2 for the stoichiometric PSMO, and the deficient $P_\square$SMO and PS$_\square$MO relaxed films. The method for determining precisely T_C is the extrapolation at $1/\chi = 0$ of the Curie-Weiss law as shown on Fig. 2c). Note that this method produces higher T_C values, than the more-often used procedure, which consists to extrapolate the tangent at the inflexion point of $m(T)$. The Curie laws for PSMO and P$_\square$SMO exhibit a similar slope reflecting similar values for both the Curie coefficient and the critical exponent. All the temperatures T_{P} and T_C values are listed in Table 2. The bulk T_C from reference [18] is also given for comparison. In our films, it is found that T_{P} and T_C are decoupled with a shift of around 30 K. Such decoupling of the transition temperatures have been often observed in thin films [22,23] and can be due to a strong disorder at T_C or to a competition between double-exchange and super-exchange of Mn-Mn spins [24]. In the following of this paper, the role of the vacancy will be discussed only

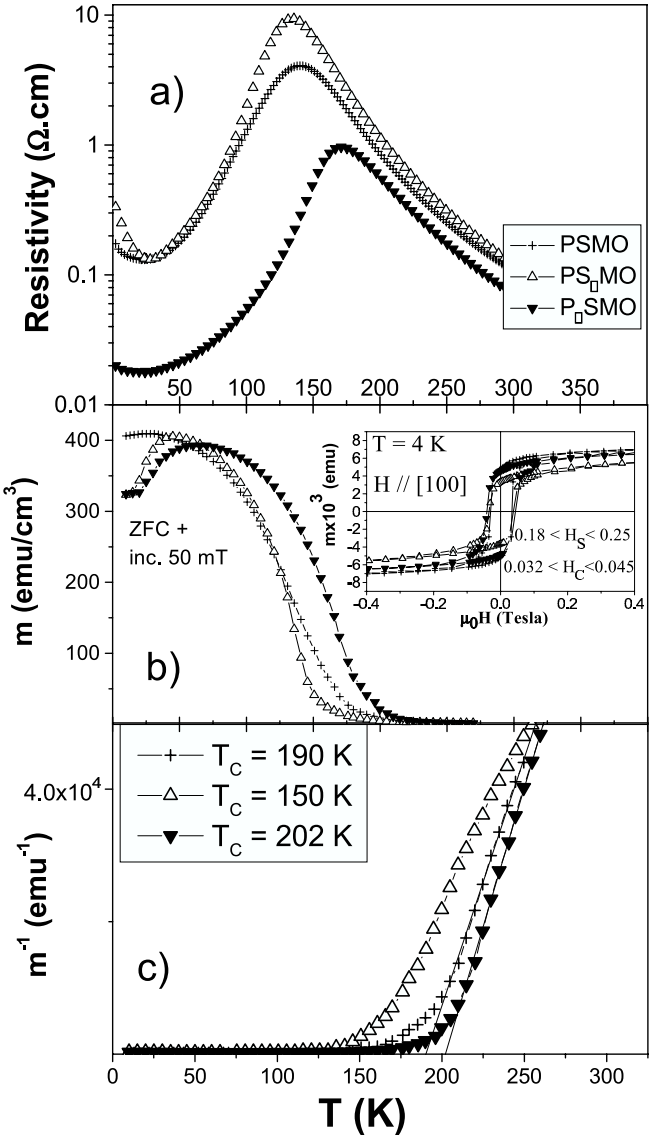

Fig. 2. a) The resistivity curves $\rho(T)$ measured using a conventional four-probe technique (the voltage contacts aligned along (100)), b) the magnetization curves $m(T)$ recorded on warming under 50 mTesla, after a zero field cooling and with the magnetic field applied along the in-plane (100) axis. The inset shows the $m(H)$ curves at 4 K where m is the magnetic moment of the samples, and c) the $1/m(T)$ curves with the high temperature Curie Weiss fits for the determination of T_C. The determined T_C values are also reported.

on the basis of the variation of T_C and the lacunars films will be directly compared to the stoichiometric PSMO film. It is not surprising to get a large decrease of T_C of around 30 K in the Sr deficient PS$_\square$MO film (see Tab. 2), since the hydrostatic ε_{B} distortion is enhanced (see Tab. 1; $\Delta\varepsilon_{\mathrm{B}} = \varepsilon_{\mathrm{B\,PS\square MO}} - \varepsilon_{\mathrm{B\,PSMO}} = 2.08 \times 10^{-3} - 1.9 \times 10^{-3} = 0.18 \times 10^{-3}$), while the Pr deficient P$_\square$SMO film exhibits an enhancement of T_C, which has to be attributed to a reduction in $\varepsilon_{\mathrm{B}}(\Delta\varepsilon_{\mathrm{B}} = -0.30 \times 10^{-3})$.

Table 2. The temperatures T_P and T_C deduced from the normalized resistivity curves $R(T)/R(300\ K)$ and the magnetization curves $m(T)$ (extrapolation at $1/\chi = 0$ of the Curie-Weiss law). The bulk T_C from reference [18] is also given for comparison.

	$Pr_{0.7}Sr_{0.3}MnO_3$	$Pr_{0.7}Sr_{0.2}\square_{0.1}MnO_3$	$Pr_{0.6}\square_{0.1}Sr_{0.3}MnO_3$
$T_{C\,\mathrm{bulk}}$ from [18]	265 K	160 K	290 K
T_P	140 K	136 K	171 K
T_C	190 K	150 K ($\Delta_{/\mathrm{PSMO\ film}} \sim -40$ K)	202 K ($\Delta_{/\mathrm{PSMO\ film}} = +12$ K)
Calculated T_C using Millis formula [19]	$\alpha = 150$	**110** K	**220** K

The expected magnetic moment at saturation for the bulk PSMO of 3.7 μ_B per formula unit is never achieved in thin films, due to the presence of magnetic "dead layers" at both substrate/film interface and air/film surface [25]. Both PSMO and $PS_{\square}MO$ films exhibit a saturation moment at 50 K of around 400 emu/cm^3 ($\sim$2.6 μ_B/f.u). Thus 70% of the film is ferromagnetic which corresponds to a ferromagnetic thickness of 420 nm. Such reduction of moment has been previously reported in thin strained PSMO films by Wu et al. [26], as well as in 700 nm-thick PSMO films by Wolfman et al. [27]. The saturation moment of the Pr deficient $P_{\square}SMO$ film is reduced to 390 emu/cm^3 in agreement with previous observations on polycrystals [21]. Note that the valence of Mn is changing in the deficient compounds: the Mn^{4+} content is always increasing with a value of 0.5 in $PS_{\square}MO$ ($Pr_{0.7}Sr_{0.2}\square_{0.1}Mn^{3+}_{0.5}Mn^{4+}_{0.5}O_3$) and of 0.6 in $P_{\square}SMO$ ($Pr_{0.6}\square_{0.1}Sr_{0.3}Mn^{3+}_{0.4}Mn^{4+}_{0.6}O_3$). The theoretical values for the saturation magnetization are thus 3.5 μ_B/f.u. ($= 2\,(3/2 \times 0.5 + 4/2 \times 0.5)$) for the $PS_{\square}MO$ compound and 3.4 μ_B/f.u. ($= 2\,(3/2 \times 0.6 + 4/2 \times 0.4)$) for $P_{\square}SMO$ [21]. In both lacunars films, the magnetization is strongly decreasing at temperatures lower than 50 K indicating a spin-canted state at low temperature, which is probably due to a pinning of the domain walls, favored by the disorder induced by the vacancies. The inset in Fig. 2b) shows the m(H) hysteresis loops recorded along the (100) in-plane direction. The stoichiometric PSMO exhibits a saturation field of about 0.18 T and a coercivity of 32 mT. It is not surprising to get a quite in-plane anisotropy in these relaxed films that are under a small tensile stress [26]. It is observed that the Sr deficient $PS_{\square}MO$ film exhibits a larger saturation field H_S of 0.25 T associated to a smaller remanent magnetization value ($m_R/m_S \sim 63\%$). The presence of disorder induced by the presence of the vacancies explains this reduction of m_R and the enhancement of H_S. Finally, no significant variation of the coercitive field is observed in the m(H) hysteresis loops due to the introduction of a vacancy: H_C is ranging from 32 mT in the PSMO film to 45 mT in the $P_{\square}SMO$. These coercivities are of the same order of those measured by Wu et al. [26] in thin strained PSMO films on STO that are under tensile stress.

4.2 Magnetoresistance

4.2.1 High Field Magneto-Resistance – HFMR

The dependence with the temperature of the High Field Magnetoresistance *HFMR*, defined as $-CMR = -[R(8T) - R(0T)]/R(8T)$, is plotted in Figure 3. In the inset, both the zero field resistance for the $PS_{\square}MO$ film and the corresponding *HFMR* curve are given for comparison. In our deficient relaxed films, it is confirmed that the maximum of *HFMR* peaks at the transition temperature, similarly as in stoichiometric manganites [13]. Also, the lowest the T_C the highest the *HFMR*, since the resistivity of the high temperature phase strongly increases on decreasing T_C, whereas that of the low temperature FM phase decreases.

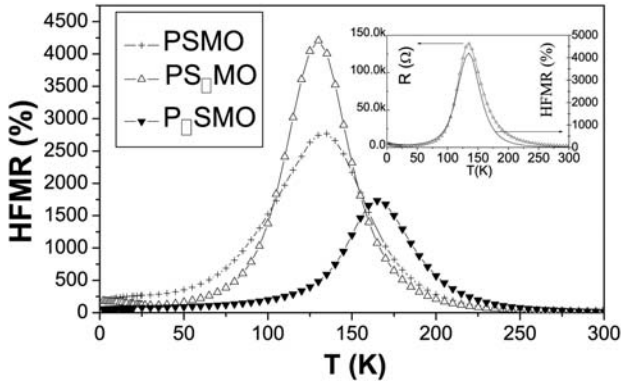

Fig. 3. The colossal magneto-resistance *HFMR(T)* curves with $HFMR(T) = -[R(8T) - R(0T)]/R(8T)$. The inset shows a comparison of both $R(T)$ and *HFMR(T)* curves of the $PS_{\square}MO$ film.

4.2.2 Low Field Magneto-Resistance – *LFMR*

The low field *MR* defined as $LFMR = [R(H) - R(H_C)]/R(H_C)$ has been also studied and its dependence is reported in Figure 4. The *LFMR*, that is related to the alignment of the ferromagnetic domains at low field, increases with decreasing the temperature and the particle size [28]. Due to its extreme sensitivity to reflect the presence of large grain boundaries, *LFMR* is often used to verify the crystallinity of the film.

In the low temperature phase at 10 K, all the films exhibit a very small *LFMR* of -5% at 0.4 Tesla and the very small slope of the curves indicates that the grains are not magnetically decoupled. The high crystallinity of our relaxed films is confirmed by this reduced slope of the *LFMR* curves. The smallest *MR* dependence with the magnetic field is obtained for the metallic $P_{\square}SMO$ that shows also the lowest resistivity ($\rho < 0.02\ \Omega\,\mathrm{cm}$ – see Fig. 2a). This is

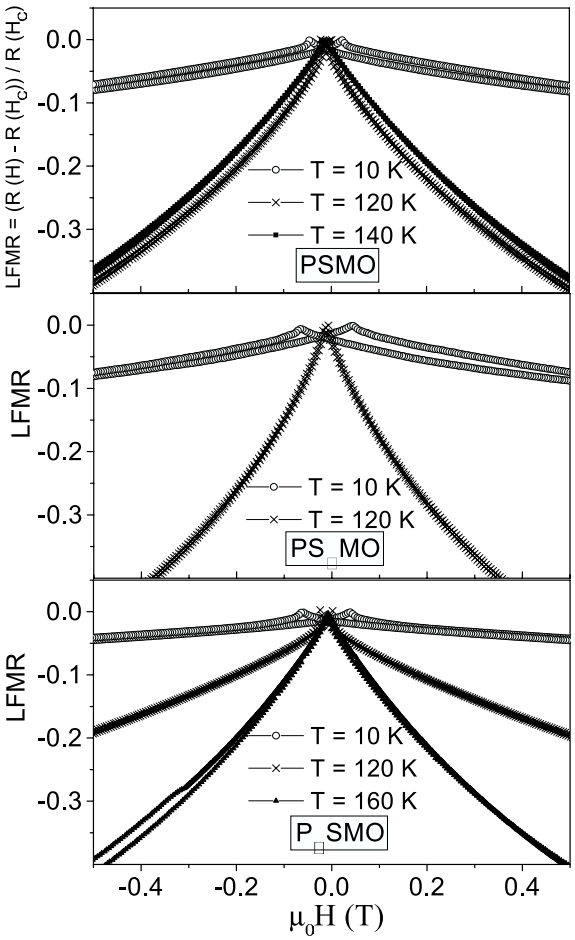

Fig. 4. The low field magneto-resistance *LFMR(T)* curves recorded at 10 K and at closer to T_P temperatures (120 K–160 K) ($LFMR = [R(H) - R(H_C)]/R(H_C)$).

the proof of the high crystallinity of this film. Moreover, it seems that the disorder, due to vacancies in the low temperature spin-canted phase, doesn't affect the *LFMR* value. In addition to an enhanced T_C, the Pr deficient P□SMO film appears more metallic, with a reduced MR sensitivity at low field.

5 Mechanism of the evolution of T_C from the vacancy

Millis et al. have developed a model in order to predict the dependence on T_C of a biaxial strain [20]. In a strained film, the 3D strain states can be decomposed into a uniform bulk strain (hydrostatic term) ε_B and a biaxial strain (Jahn-Teller term) ε_{J-T} [20]. These compounds have opposite effects upon T_C. An hydrostatic compression ($\varepsilon_B < 0$) will tend to increase the hopping and thereby reduce the electron-lattice coupling, inducing an increase in both the conduction band width and T_C. On the other hand, a biaxial strain ε_{J-T} increases the energy differences between the e_g levels imposed by the Jahn-Teller, which reinforce the electrons tendency to become more localized decreasing T_C. The Curie temperature dependence can be expressed in powers of the strains as:

$$T_C(\varepsilon_B, \varepsilon_{J-T}) = T_C(0,0) \times \left[1 - \left[\frac{1}{T_C(0,0)}\frac{dT_C}{d\varepsilon_B}\right]\varepsilon_B - \left[\frac{1}{2T_C(0,0)}\frac{d^2T_C}{d\varepsilon_{J-T}^2}\right]\varepsilon_{J-T}^2\right] \quad (1)$$

$$\text{or} \quad T_C(\varepsilon_B, \varepsilon_{J-T}) = T_C(0,0)(1 - \alpha\varepsilon_B - 1/2\Delta\varepsilon_{J-T}^2) \quad (2)$$

where α and Δ represent respectively the relative weight of the bulk-strain ε_B and of the biaxial strain (Jahn-Teller term) ε_{J-T}. In very thin strained films, the ε_{J-T} term is more often negligible, the ε_B term being the most important one. This ε_B term is related to the variation of the kinetic energy of the carriers with respect to the stress. A tensile strain ($\varepsilon_B > 0$) generally induces a decrease in T_C, because the transfer of carriers in the film's plane is decreased due to stretched Mn-O bonds. On the opposite a compression with a negative ε_B term will enhance T_C. This has been confirmed experimentally for (La,Ca)MnO_3, (La,Sr)MnO_3 and (Pr,Sr)MnO_3 thin strained films deposited on different substrates [13].

In this study, by depositing thick relaxed films in which both ε_B and ε_{J-T} terms are of the same order, i.e. several 10^{-3} (see Tab. 1), the second bulk-strain ε_B term in the equation (2) is largely reduced compared to what is usually observed in thin strained films. Thus, the ε_{J-T} term has to be taken in account for the prediction of T_C. As previously mentioned, ε_B and ε_{J-T} are not varying similarly with the nature of the vacancy. With a Sr vacancy, ε_B is enhanced producing a larger second term in the equation (2) and T_C is thus decreased. On the opposite, a Pr vacancy induces a more significant decrease of both ε_B (reduced from 13%) and ε_{J-T} (divided by 5) distortions. This reduces simultaneously the second ε_B and third ε_{J-T} terms in the equation (2), which enhances T_C. We tried to apply numerically the model of Millis to predict T_C of the lacunars films. We have taken $\Delta = 500$ from reference [16] and $T_C(0) = 265$ K from reference [18] for the stoichiometric compound PSMO. The resolution of equation with our experimental T_C value of 190 K in the thick relaxed PSMO film gives $\alpha = 150$. Millis equation (2) becomes:

$$T_C(\varepsilon_B, \varepsilon_{J-T}) = T_C(0,0)(1 - 150\varepsilon_B - 250\varepsilon_{J-T}^2). \quad (3)$$

Using this equation (3), the calculated T_C for PS□MO and P□SMO films are respectively 110 K and 220 K, whereas the experimental values are 150 K and 202 K (see Tab. 2). T_C appears not predictable with a precision better than 20 K [29], probably because of the lack of precision for both α and Δ parameters, as well as because this equation does not take in account the change of Coulomb disorder in the deficient compounds. However, the tendency is well reproduced proving that the role of both strains can be roughly predicted from the model. Our measurements in thick relaxed films show a similar T_C dependence with the nature of the vacancy than the one previously observed in

bulk polycrystalline materials [17,18]. Our next goal will be now to stabilize thin epitaxial strained films in which both substrate lattice mismatch strain and vacancy strain will compete. In those thin strained films on LAO, and more particularly in the Pr deficient $P_{\square}SMO$ compound, one should expected a reduction of the cell volume, associated to a reduction of the out-plane parameter that should decrease the total film strain.

6 Conclusion

In summary, the introduction of cationic vacancies in thick relaxed PSMO films has been shown to affect the strains. Similarly to polycrystalline $P_{\square}SMO$ and $PS_{\square}MO$ compounds, a decrease of the unit cell due to the presence of cationic vacancies was observed. However, the calculated strains, ε_{B} and $\varepsilon_{\mathrm{J-T}}$, are not varying similarly with the nature of the vacancy. A Sr vacancy enhanced ε_{B} while, on the opposite, a Pr vacancy reduces the out-plane cell distortion, inducing a more significant decrease of both ε_{B} and $\varepsilon_{\mathrm{J-T}}$ distortions.

A direct correlation upon T_C of these strains has also been observed. In the Sr deficient $PS_{\square}MO$ thick film, the Curie temperature T_C decreases of 30 K ($\Delta\varepsilon_{\mathrm{B}} = 0.18 \times 10^{-3}$), while the Pr deficient $P_{\square}SMO$ film exhibits a 12 K enhancement of T_C ($\Delta\varepsilon_{\mathrm{B}} = -0.30 \times 10^{-3}$). The high saturation moment at low temperature associated with a low *LFMR* demonstrates that those deficient films are well crystallized. With a reduced resistivity ($\rho < 0.02\ \Omega\,\mathrm{cm}$), the Pr deficient $P_{\square}SMO$ film exhibits the best magneto-transport properties with a reduced MR sensitivity at low field ($LFMR_{10\ \mathrm{K}-0.4\,\mathrm{T}} < 4\%$).

These results indicate that the introduction of cationic vacancies can be an alternated method to change the physical properties of manganite thin films that can be used for other oxide films.

We wish to thank J.P Renard, C. Dupas, and B. Mercey for fruitful scientific discussions. This work was supported by the "Comité Mixte Franco-Tunisien" CMCU 02/F-11-16 project.

References

1. R.M. Kusters, J. Singleton, D.A. Keen, R. McGreevy, W. Hayes, Physica B **155**, 362 (1989)
2. R. von Helmolt, J. Wecker, B. Holzapfel, L. Schultz, K. Samwer, Phys. Rev. Lett. **71**, 2331 (1993)
3. K. Chahara, T. Ohno, M. Kasai, Y. Kozono, Appl. Phys. Lett. **63**, 1990 (1993)
4. S. Jin, T.H. Tiefel, M. Mc Cormack, R.A. Fastnacht, R. Ramesh, L.H. Chen, Science **264**, 413 (1994)
5. A.J. Millis, P. Mueller, B.I. Shraiman, Phys. Rev. B **54**, 5389 (1996)
6. A.J. Millis, P. B. Littlewood, B. I. Schraiman, Phys. Rev. Lett. **74**, 5144 (1995)
7. A. Sundaresan, A. Maignan, B. Raveau, Phys. Rev. B **56**, 5092 (1997)
8. G. Zhao, K. Conder, H. Keller, K.A. Müller, Nature **381**, 676 (1996)
9. N.A. Babushkina, L.M. Belova, O. Yu Gorbenko, A.R. Kault, A.A. Bosak, V.I. Ozhogin, K.I. Kugel, Nature **391**, 159 (1998)
10. P. Postorino, A. Congeduti, P. Dore, A. Sacchetti, F. Gorelli, L. Ulivi, A. Kumar, D.D. Sarma, Phys. Rev. Lett. **91**, 175501-1 (2003)
11. V. Laukhin, J. Fontcuberta, J.L. Garcia-Munoz, X. Obradors, Phys. Rev. B **56**, R10 009 (1997)
12. P.G. Radaelli, G. Iannone, M. Marezio, H.Y. Hwang, S.W. Cheong, J.D. Jorgensen, D.N. Argyriou, Phys. Rev. B **56**, 8265 (1997)
13. For detailed recent reviews of the works on manganite thin films: A.M. Haghiri-Gosnet, J.P. Renard, J. Phys. D: Appl. Phys. **36**, R127 (2003); W. Prellier, B. Mercey, A.M. Haghiri-Gosnet, *Encyclopedia of Nanoscience and Nanotechnology*, edited by H.S. Nalwa, Vol. X (2003), p. 107, J.Z. Sun, L. Krusin-Elbaum, A. Gupta, G. Xiao, P.R. Duncombe, S.S.P. Parkin, IBM J. Res. Develop. **42**, 89 (1998)
14. T. Kanki, H. Tanaka, T. Kawai, Phys. Rev. B **64**, 224418 (2001)
15. H.S. Wang, Qi Li, Appl. Phys. Lett. **73**, 2360 (1998)
16. H.S. Wang, E. Wertz, Y.F. Hu, Qi Li, D.G. Schlom, J. Appl. Phys. **87**, 7409 (2000)
17. W. Boujelben, A. Cheikh-Rouhou, J. Pierre, D. Abou-Ras, J.P. Renard, K. Shimizu, Physica B **321**, 68 (2002)
18. D. Abou-Ras, W. Boujelben, A. Cheikh-Rouhou, J. Pierre, J.P. Renard, L. Reversat, K. Shimizu, J. Magn. Magn. Mater. **233**, 147 (2001)
19. K. Knizek, Z. Jirak, E. Pollert, F. Zounova, S. Varstislav, J. Solid State Chem. **100**, 292 (1992)
20. A.J. Millis, T. Darling, A. Migliori, J. Appl. Phys. **83**, 1588 (2000)
21. W. Boujelben, A. Cheikh-Rouhou, J. Pierre, J.C. Joubert, Physica B **321**, 37 (2002)
22. J. Aarts, S. Freisem, R. Hendrikx, H.W. Zandbergen, Appl. Phys. Lett. **72**, 2975 (1998)
23. R.A. Rao, D. Lavric, T.K. Nath, C.B. Eom, L. Wu, F. Tsui, J. Appl. Phys. **85**, 4794 (1999)
24. A.K. Heilman, Y.Y. Xue, B. Lorenz, B.J. Campbell, J. Cmaidalka, R.L. Meng, Y.S. Wang, C.W. Chu, Phys. Rev. B **65**, 214423 (2002)
25. R.P. Borges, W. Guichard, J.G. Lunney, J.M.D. Coey, F. Ott, J. Appl. Phys. **89**, 3868 (2001)
26. X.W. Wu, M.S. Rzchowski, H.S. Wang, Q. Li, Phys. Rev. B **61**, 501 (2000)
27. J. Wolfman, W. Prellier, Ch. Simon, B. Mercey, J. Appl. Phys. **83**, 7186 (1998)
28. A. Gupta, J.Z. Sun, J. Magn. Magn. Mater. **200**, 24 (1999)
29. M. Bibes, S. Valencia, L.I. Balcells, B. Martinez, J. Fontcuberta, M. Wojcik, S. Nadolski, E. Jedryka, Phys. Rev. B **66**, 134416 (2002)